An integrated 9x9 SPAD array with a 10-channel TDC and a CMOS laser diode driver for a wearable time-domain diffuse optics optode

1st Jussi-Pekka Jansson
Circuits and Systems Research Unit
University of Oulu
Oulu, Finland
jussi.jansson@oulu.fi

2nd Sahba Jahromi
Circuits and Systems Research Unit
University of Oulu
Oulu, Finland
sahba.jahromi@oulu.fi

3th Kalle Haapalainen
Circuits and Systems Research Unit
University of Oulu
Oulu, Finland
kalle.haapalainen@oulu.fi

4th Harri Juttula
Optoelectronics and Measurement Techniques Research Unit
University of Oulu
Oulu, Finland
harri.juttula@oulu.fi

5th Anssi Mäkynen
Optoelectronics and Measurement Techniques Research Unit
University of Oulu
Oulu, Finland
anssi.makynen@oulu.fi

6th Jan Nissinen
Circuits and Systems Research Unit
University of Oulu
Oulu, Finland
jan.nissinen@oulu.fi

***Abstract*—A 9x9 Single-Photon Avalanche Photodiode (SPAD) array with a 10-channel time-to-digital converter and an integrated laser diode driver fabricated in 0.35 µm HV-CMOS technology were used to carry out time domain diffuse optics measurements of optical phantoms. The average optical power of 20 µW was achieved by the laser diode transmitter at the repetition rate of 500 kHz with a pulse width of 80 ps. The resolution of the TDC and the measured instrument response function (IRF) of the system were ~65 ps and ~190 ps, respectively. The power consumption of the proposed system was 180 mW. Measurements showed that with the proposed system a perturbation with a different absorption property than in surrounding material at the depth of 15 mm could be recognized. In addition, in *in vivo* measurement with the proposed components, hemodynamic changes in volunteer's arm during a venous occlusion were detected.**

Keywords—Diffuse optics, Time-correlate single photon counting, laser diode, time-to-digital converter, NIRS

I. INTRODUCTION

Diffuse optics imaging has proven a promising method for characterizing diffusive media such as biological tissue, wood or chemical compounds [1]. Moreover, the used wavelength of the visible or near-infrared range, so called therapeutic window (600 nm-1000 nm), makes non-ionizing and non-invasive probing of a tissue possible. The used wavelength range enables to probe deep in a tissue because the absorption of the most biological media is low and the interaction between photons and turbid media is dominated by scattering. There are also commercial wearable diffuse optics systems on the market for the personal monitoring of muscle oxygenation during physical exercise [2]. Yet, systems are based on a traditional continuous-wave (CW) or frequency-domain principle because of the compact size of the components operating in such domains. Moreover, with the traditional continuous-wave (CW)-based structure only the relative changes of the absorption (μ_a) and reduced scattering coefficient (μ_s') can be solved because the measurement enables only the evaluation of the changes of the light intensity. In addition, to probe deeper into the tissue, the distance between the source-detector pair (ρ in top of Fig. 1 b)) has to be increased with the CW-based structure in which case the signal-to-noise ratio is degraded.

Contrary to the CW system, time-domain (TD) diffuse optics systems benefit from their unique feature to select depths to be probed by the times of arrival of the back scattered photons. In other words, the later the photon is detected the deeper it has penetrated so that the selection of the probed depths can be verified in the time domain. Fortunately, optical properties of the investigated medium can be directly solved from the DTOF in which case the distance between the detector and the source can be kept as short as possible. Thus, even in an ideal case physics itself limits the achievable penetration depth of the CW device to be lower than in an ideal TD system so that a higher signal-to-noise ratio can be achieved when the TD system is used [3].

The TD diffuse optics measurement is based on a pulsed laser transmitter, which emits a short optical pulse to a turbid medium (e.g., muscle, brain or breast), and back scattered light is detected by a time-resolved single-photon detector. By means of time-correlated single-photon counting (TCSPC) electronics, the distribution of photon time-of-flight (DToF) can be defined. The instrument response function of the laser, DToF of detected photons and the measurement principle in a reflectance geometry are shown in Fig. 1 a) and b), respectively. The shape of the DTOF can be used to evaluate the absorption and scattering properties of the tissue [4]. As can be seen in Fig. 1 a) and b), perturbation having a higher absorption coefficient than the surrounding material will decrease the amount of photons detected later in relation to the depth of the perturbation.

During past decades, a lot of research has been done to scale down the size of components such as pulsed laser diode drivers, photo detectors and time correlated single photon counting electronics needed for TD diffuse optics systems to fabricate a small-sized wearable optode [3,5]. From the detector point of view, the solid-state detector such as a SPAD or SPAD array is very promising because it can be integrated with timing electronics in CMOS technology to fabricate a compact sensor circuit into a single die [6]. Moreover, the SPAD has a good single-photon sensitivity and a short inherent timing jitter (50-100 ps) when biased over the breakdown voltage to the so-called Geiger mode.

From source point of view the main bottleneck has been to fabricate a small-sized laser diode driver which can produce enough power within a short optical pulse width of 100 – 200 ps. The semiconductor laser diode with a CMOS driver of 6 mm x 12 mm in size has been presented for TD diffuse optics together with a commercial Silicon photomultiplier (SiPM)

This work was supported by the Academy of Finland under contracts 314404 and 323719 and (Centre of Excellence in Laser Scanning Research) under Contract 307362.

and a TCSPC board [7] and also some preliminary measurements have been carried out with a CMOS single-photon avalanche diode and the same laser diode driver and a rack-sized time-to-amplitude converter (ORTEC TAC 566) in [8]. In [9], an eight wavelength time-resolved diffuse optical spectroscopy system has been presented which uses eight laser diodes at different wavelengths in the near-infrared region, two custom-made SiPMs and two custom-made time-to-digital converters (TDC) fabricated on 0.35 µm HV-CMOS technology. However, the system is targeted for clinical use and the size of the system is 48x38x20 cm^3. Thus, to take full advantage of CMOS technology, both a SPAD detector array and a TDC should be integrated into the same die so that a wearable optode for TD diffuse optics would be feasible. In [10], a wearable optode with a time-gated single-photon avalanche diode (SPAD) fabricated in 0.35 µm CMOS technology and a pulsed vertical cavity surface emitting laser (VCSEL) has been presented. The size of the presented optode is 12 mm x 12 mm and the FWHM of the laser is 350 ps. Unfortunately, no distribution of the photon time-of-flight (DToF) measurements of the turbid media have been presented to prove the functionality in a real environment.

In this work both the 9x9 SPAD array with a 10-channel TDC and the CMOS driver with a quantum well laser diode fabricated in 0.35 µm HV-CMOS technology were used to carry out a TD diffuse optics measurement to recognize perturbation inside a homogenous background. In addition, *in vivo* measurement was carried out to prove the feasibility of the system for detecting hemodynamic changes in volunteer's arm during a venous occlusion.

II. TD DIFFUSE OPTICS MEASUREMENT ARCHITECTURE

A simplified block diagram of the used time domain diffuse optics measurement system in reflectance geometry is shown in Fig. 2 a). The quantum well laser diode (LD in fig. 2 a) with a CMOS driver has been used as a source which emits ~800 nm optical pulse of 80 ps (FWHM). The detailed structure of the laser diode and the CMOS driver can be found in [11,12]. The time-gated 9x9 SPAD array with 10-channel TDC has been used as a sensor (Receiver IC in Fig. 2a) [13]. Both the laser diode driver and SPAD array have been fabricated in 0.35 µm HV-CMOS technology and the photographs of both chips and the laser diode transmitter are shown in Fig. 2 b). Because both the transmitter and the receiver have been designed on their own test PCBs, optical fibres (core diameter of 105 µm) have been used to guide the optical signal from the laser diode to the phantom and then back to the receiver so that the electrical delay of the synchronization signal from the laser to the receiver could be cancelled.

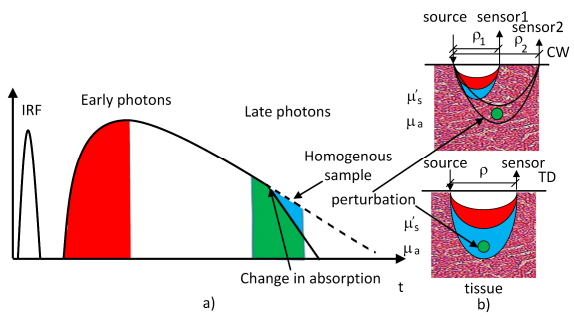

Fig. 1. a) IRF of the laser and distribution of the time-of-flight in a TRDOI measurement, and b) the principle of TRDOI measurement.

A. SPAD receiver

The SPAD is based on a deep-nwell cathode and a p+ anode with a pwell guard ring [13]. The active area of each square SPAD with rounded corners is 24 µm x 24 µm. The designed receiver consists of 9x9 SPAD array which can be divided to 3x3 sub-arrays so that each SPAD of a sub-array can trigger one of the channels of the TDC. Thus, the size of the active area of the selected sub-array is 72 µm x 72 µm with a fill factor of 51.4%. Each SPAD of the selected sub-array can be actively enabled by the synchronization signal (Sync. in Fig. 2a)) from the laser so that SPADs are ready to detect photons after the optical pulse is transmitted to the investigated medium. Moreover, the start signal for the TDC is generated simultaneously.

The front-end electronics of SPADs is shown in Fig. 3. The cathode of the SPAD is connected to high voltage (V_{HV}) which is ~3.3 V (V_{dd} of the technology) larger than the breakdown voltage of the SPAD and it is the excess bias voltage of the SPAD. The SPADs of the selected sub-array are enabled by the EN signal. In the beginning of a measurement cycle, the quench signal is low and anodes of the SPADs are 3.3 V and they cannot detect photons. After that the quench signal is set high so that the anode is floating. In the next phase, the Load signal is set high and the anode is discharged to ground by the transistor M1 so that SPADs are ready to detect photons as illustrated in the timing diagram in Fig. 3 b). When a photon is detected, the anode of a SPAD rises to the V_{DD} and simultaneously a stop timing mark is generated for a TDC.

The 10-channel TDC, based on a counter and delay line interpolation using two nested levels at a different resolution, can measure intervals between the start and 9 stop timing signals from the selected 3x3 SPAD sub-array. The resolution of the TDC is locked by a delay-locked loop to the reference crystal so that fluctuations caused by process, voltage and temperature variations can be avoided. The LSB and measurement range of the TDC used in measurements are 65.1 ps and 533 ns, respectively. The power consumption of the receiver is approximately 150 mW. Detailed information about the TDC can be found in [14].

B. Laser diode transmitter

A compact laser transmitter based on quantum well laser diode, which operates on the "enhanced gain switching" principle, and a CMOS driver was used as a source [11,12]. The laser diode can produce short optical pulses of ~80 ps (FWHM) when driven with a current pulse width of ~1 ns and a peak amplitude of a few amperes.

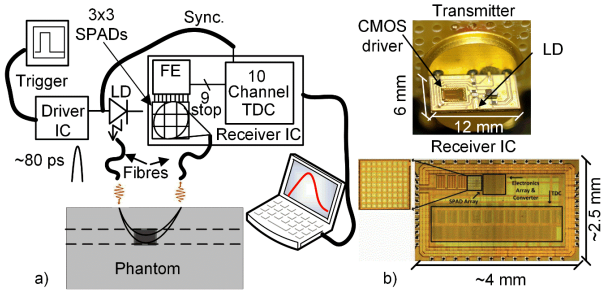

Fig. 2. a) The developed TD diffuse optics measurement system and b) aphotograph of the pulsed laser diode transmitter and the receiver chip with a SPAD array and 10-channel TDC.

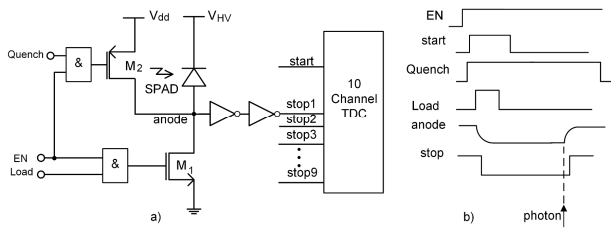

Fig. 3. a) The front-end electronics of the receiver and b) timing diagram of the signals.

A laser diode driver designed in 0.35 µm HV-CMOS technology is based on an LC-transient pulse shaping, as shown in Fig. 4. At the beginning, the capacitor C_1 is charged to 20 V through the resistor R_b and the Schottky diode D when the switch M_1 is open. The switch transistor M_1 is turned on by the rising edge of the trigger signal in which case the laser diode is forward biased because the charge of the capacitor cannot change instantaneously. Thus, a current starts to flow through the RLC branch simultaneously discharging the capacitor C_1. The width of the current pulse can be defined by the capacitor C_1 and the total inductance of the loop and the proper damping of the oscillation is achieved by the resistor R_d as explained in more detail in [12].

The start timing mark for the TDC is generated from the current pulse through the laser diode and the resistor R_d. The optical peak power and pulse width (FWHM) of a laser diode at the used bias voltage of 20 V were approximately 1 W and ~80 ps, respectively. The power consumption of the transmitter was approximately 30 mW at the repetition rate of 500 kHz.

III. Measurements

To measure DToF of back scattered photons from a turbid medium, the synchronization signal (sync. in Fig. 2) from the laser driver enables SPADs and simultaneously gives a start timing mark for the TDC. Now SPADs are ready to detect back scattered photons from the turbid medium. Thus, any of the SPADs of the 3x3 SPAD array can be triggered by the photon and give a stop timing mark (9 stop in Fig. 2) to the TDC. After that the time interval measurement result can be transferred out of the chip and a next laser pulse can be triggered. Results from all 9 TDC channels are combined to one DToF result after the measurement. The photon detection probability was kept below 10% so that the single-photon level could be guaranteed in measurements.

A. Instrument response function (IRF) measurement

Before the time domain diffuse optics measurement of the phantom, the IRF of the measurement setup was measured to evaluate the total jitter of the time domain diffuse optics system developed here. The IRF of the whole system is shown in Fig. 5 and FWHM of the IRF was approximately 190 ps.

B. DToF of the phantom

To prove the feasibility of the TD diffuse optics system, commercial biomimic optical phantom (polyurethane n=1.52) with absorption and reduced scattering coefficients of 0.04 cm^{-1} and 9.74 cm^{-1} at 800 nm was used in the measurements. The setup shown in Fig. 2 was used in DToF measurements in reflectance geometry with the source-detector distance of 18 mm. The repetition rate of the laser diode was 500 kHz, and 15 000 000 pulses were transmitted to the phantom. The average optical power was approximately 20 µW. The DToF of the homogenous phantom is shown in Fig. 6 (blue line).

To solve the values of the μ_a and μ_s' from the measured DToF, an analytical solution of the radiative transport equation under the diffusion approximation was convoluted with the instrument response function of the setup and then fitted to the measured DToF [15]. According to the above principle, the μ_a and μ_s' were defined to be 0.063 cm^{-1} and 13.6 cm^{-1}, respectively. The difference between the measured and the real values can be explained by the moderate resolution of the TDC (65 ps) and the timing skew of the different SPADs so that the timing and the shape of the peak of the IRF could not be exactly defined.

C. Perturbation measurement

With the same setup used in the measurement of the homogenous phantom, the capability to detect a perturbation buried inside a homogenous background was tested. For this measurement, a switchable solid phantom was used, where an absorbing perturbation could be moved along one direction, as shown in Fig. 7 a). The background phantom has the same optical properties (0.04 cm^{-1} and 9.74 cm^{-1}) as described in the previous section while the perturbation has the absorption coefficient of 0.12 cm^{-1} (three times larger than background 0.04 cm^{-1}) in a volume of 0.79 cm^3. The perturbation was placed at the depth of 15 mm from the surface and below the axis of the source-detector pair as shown in Fig. 7 b). In Fig. 6 the DToFs of both the homogenous phantom (blue line) and the phantom with the perturbation (orange line) are shown. As can be seen in Fig. 6, the DToF curve of the phantom with the perturbation starts to decay with a steeper slope after a short delay by means of the larger absorption of the photon at the depth of the perturbation of 15 mm.

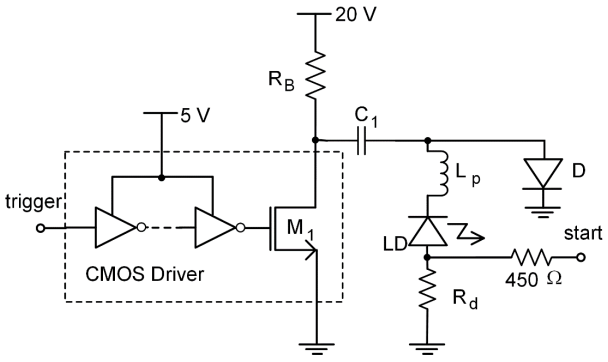

Fig. 4. The CMOS driver of the quantum well laser diode.

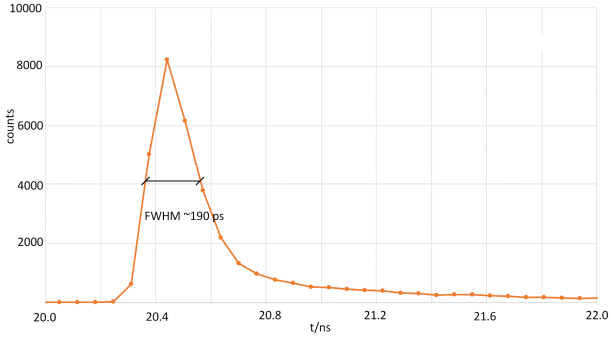

Fig. 5. The IRF of the used measurements setup.

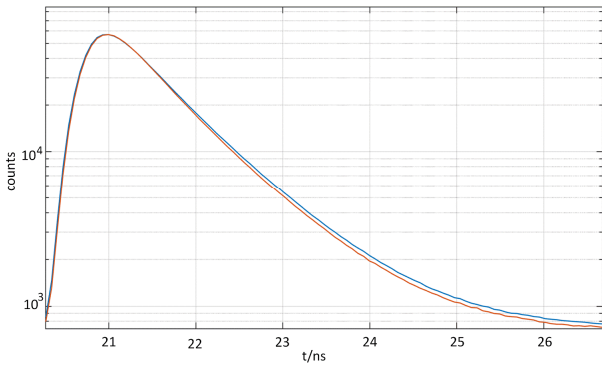

Fig. 6. The DToFs of the homogenous (blue) and phantom with a perturbation (orange).

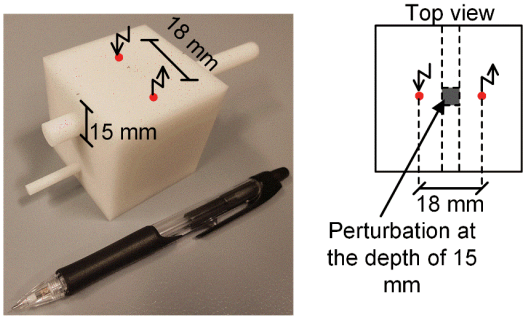

Fig. 7. a) The used optical phantom with a switchable phantom and b) a top view of the phantom with a perturbation.

To prove the developed system to recognize the perturbation at the depth of 15 mm, we used contrast (C) and contrast-to-noise ratio (CNR) tests defined in the "nEUROPt protocol"[16]. Both the contrast and the CNR were calculated by dividing the DToF in time windows. The contrast was calculated by summing up the photons detected by the 3x3 SPAD array within selected time bins (t_{BINS}) of the TDC as

$$C(t_{BINS}) = \frac{N_0(t_{BINS}) - N_P(t_{BINS})}{N_0(t_{BINS})} \quad (1)$$

where N_0 are the photons detected in homogenous case and N_P the photons detected with the perturbation within the selected time bins (t_{BINS}) of the TDC. Seven different time window positions were selected at the falling edge of the DToF so that the first one started at 456 ps after the peak of the IRF of the setup and the other ones at a delay of 456 ps from the previous one so that the last one started at a delay of 3190 ps with respect to IRF. The width of the time window was in all cases seven time bins of the TDC which is 7*65.1 ps=456 ps, as shown in Fig. 8.

For CNR, the equation given in [16] was used

$$CNR = \frac{\Delta N(t_{BINS})}{\sigma[N_0(t_{BINS}]} = \frac{N_0(t_{BINS}) - N_P(t_{BINS})}{\sigma[N_0(t_{BINS}]} \quad (2)$$

Where ΔN was calculated over 40 repetitions using same time windows as in the case of contrast calculation. The denominator $\sigma[N_0(t_{BINS})]$ was the standard deviation of the counts summed in the homogenous sample of the 40 repetitions. The contrast and CNR of the perturbation at the depth of 15 mm as a function of the time window position are shown in Fig. 9 a) and b), respectively. A threshold for detectability of perturbation can be considered to be CNR=1. Thus, with the time window starting at 1368 ps the CNR is larger than 1 (CNR=1.8 at 1368 ps) as can be seen in Fig. 9 b). Due to the depth of the perturbation (15 mm) and the selected source-detector pair distance (18 mm) the visibility of the perturbation increases with longer delays due to the longer path length of the photon travelled from the surface to an inclusion and back to the receiver. Moreover, the shortest time window position (456 ps) is collecting only the photons which have travelled through the superficial layer of the phantom and which have not reached the inclusion.

D. Preliminary In Vivo measurement

As a proof of concept of the proposed integrated SPAD receiver with a 10-channel TDC and integrated CMOS driver with a semiconductor laser diode, a preliminary *in vivo* measurement of venous occlusion was carried out. In the measurement, the same protocol was used as the phantom measurement. The separation between the detector and source fiber was selected to be 18 mm, in which case the single-photon signal level on the detector could be achieved.

Before the occlusion measurement, the diastolic and systolic blood pressure of the volunteer was defined. During the measurement, a sphygmomanometer cuff, placed on the upper arm of the subject, was used to achieve the pressure level between the diastolic and systolic ones of the volunteer so that the complete venous block could be ensured. The measurement cycle was divided into three parts. At the beginning, the baseline was measured without occlusion for 30 s. The baseline was followed by 60 s of occlusion, and a final recovery phase was 55 s so that a total measurement time of 145 s was achieved.

To demonstrate that the developed system can recognize the change of the blood volume during the occlusion, the contrast defined in (1) was calculated. More precisely, N_0 and N_p were the mean counts detected during the 30 s baseline without occlusion and counts detected every 5 s throughout the whole 145 s, respectively. The opening of the time window was selected to be 912 ps after the peak of the IRF, and the width of the time window was 456 ps.

Contrasts as a function of time, calculated every 5 s are shown in Fig. 10. During the occlusion (grey in Fig. 10), the contrast starts to increase as expected because the absorption increases due to the increased blood volume. On the other hand, the contrast recovered to a basic level when the occlusion was removed. Moreover, due to the wavelength of the laser (~800 nm), which is close to the isosbestic point of the oxygenated and deoxygenated blood, the total blood volume is sensed. In other words, the selected pressure of the sphygmomanometer cuff blocks only the venous blood flow while the arterial blood flow can continue. Thus, the blood volume is increased.

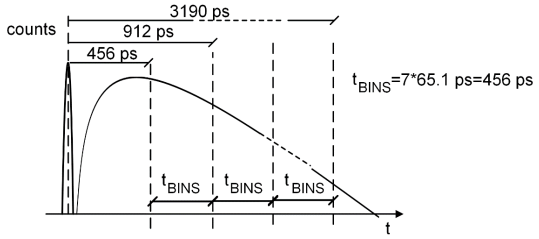

Fig. 8. The used time windows in contrast and CNR calculations.

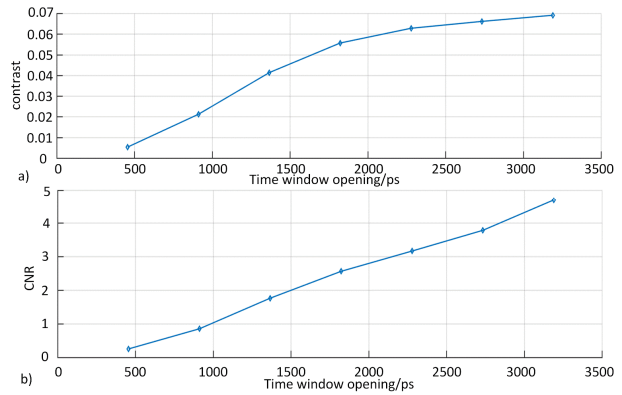

Fig. 9. a) The contrast and the b) CNR of the detectability of the perturbation at the depth of 15 mm as a function of seven different time window positions.

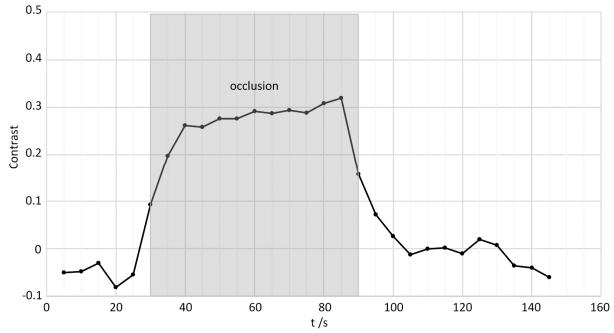

Fig. 10. Contrasts in occlusion measurement *in vivo*.

IV. CONCLUSIONS

During the last decade, a lot of research has been carried out to fabricate a small-sized optode for a time domain diffuse optics system. In this paper both the laser diode transmitter and the receiver fabricated in 0.35 µm HV-CMOS technology have been used in time domain diffuse optics measurements of a biomimic optical phantom. A 9x9 SPAD receiver with a 10-channel TDC were used as a sensor circuit to detect back scattered photons from the turbid medium and to record the timing stamps of the photons with a resolution of 65 ps. The size of the active area of the 3x3 SPAD array used in the measurements was 72 µm x 72 µm. The IRF of the TD diffuse optics measurement setup was 190 ps with the used optical pulse width of 80 ps at 800 nm.

To prove the detectability of the perturbation inside the homogenous sample, a biomimic optical phantom with a movable inclusion at the depth of 15 mm was measured. The measurement showed that with the proposed setup, the perturbation, which has three times larger absorption coefficient than a homogenous background (0.12 cm^{-1} vs. 0.04 cm^{-1}), could be recognized.

To validate the proposed integrated receiver and the laser diode driver with a quantum well laser diode for *in vivo* measurement, a venous occlusion test was carried out. The proposed measurement setup could recognize signal changes according to altered blood flow during occlusion.

Due to the small size of both the receiver IC (2.5 mm x 4 mm) and the transmitter IC with a laser diode (6 mm x 12 mm), this technology makes it possible to fabricate the transceiver optode with the size of the commercial CW based diffuse optics systems. Moreover, the advantages of the TD system compared to CW systems, such as higher penetration depth in tissue, reduced sensitivity to motion artifacts and possibility to separate absorption from scattering as well as the low power consumption of the integrated circuits of ~180 mW, will pave the way for the fabrication of small-sized wearable TD diffuse optics optodes for applications in the medical and health care sectors.

REFERENCES

[1] A. Pifferi et al."New frontiers in time-domain diffuse optics, a review," Journal of Biomedical Optics, vol.21, no. 9, Art no. 091310, 2016.

[2] P. Farzam, Z. Starkweather and M. A. Franceschini, "Validation of a novel wearable, wireless technology to estimate oxygen levels and lactate threshold power in the exercising muscle," Physiological Reports, vol.6, no.7, e13664, 2018.

[3] A. Dalla Mora et al., "Towards next-generation time-domain diffuse optics for extreme depth penetration and sensitivity," Biomedical Optics Express, Vol.6, no.5, pp. 1749-1760, 2015.

[4] M.S. Patterson, B. Chance and B.C. Wilson,"Time resoved reflectance and transmittance for the non-invasive measurement of tissue optical properties," Appl. Opt., 28(12), pp.2331-2336, 1989.

[5] H. Zhao, F. Gao, Y. Tanikawa and Y. Yamada, "Time-resolved diffuse optical tomography and its application to in vitro and in vivo imaging," Journal of Biomedical Optics, vol.12, no.6, 062107, 2007.

[6] J. M. Pavia, M. Scandini, S. Lindner, M. Wolf and E. Charbon, "A 1x400 Backside-illuminated SPAD Sensor with 49.7 ps Resolution, 30 pJ/Sample TDCs Fabricated in 3D CMOS Technology for Near-Infrared Optical Tomography," IEEE Journal of Solid-State Circuits, vol.50, no.10, pp.2406-2418, 2015.

[7] L. Di Sieno et al., "Miniaturized pulsed laser source for time-domain diffuse optics routes to wearable devices," Journal of Biomedical Optics, vol.22, no.8, 085004, 2017.

[8] J. Nissinen, I. Nissinen, S. Jahromi, T. Talala and J. Kostamovaara, "Time-gated CMOS SPAD and a Quantum Well Laser Diode with a CMOS Driver for Time-Resolved Diffuse Optics Imaging," in Proc. IEEE NORCAS, Estonia, Tallinn, 30-31 Oct. 2018.

[9] M. Renna et al.," Eight-Wavelenght, Dual detection Channel Instrument for Near-Infrared Time-Resolved Diffuse Optical Spectroscopy," IEEE Journal of Selected Topics in Quantum Electronics, vol.25, no.1, 7201611, 2019.

[10] S. Saha, Y. Lu, S. Weyers, M. Sawan and F. Lesage, "Compact Fast Optode-Based Probe for Single-Photon Counting Applications," IEEE Photonics Technology Letters, vol.30, no.17, pp.1515-1518, 2018.

[11] B. Ryvkin, E. A. Avrutin and J. T. Kostamovaara, " Asymmetric-waveguide laser diode for high-power optical pulse gneration by gain switching," IEEE Journal of Lightwave Technology, vol.27, no. 12, pp.2125-2131, 2009.

[12] J. Nissinen and J. Kostamovaara,"A High Repetition Rate CMOS Driver for High-Energy Sub-ns Laser Pulse Generation in SPAD-Based Time-of-Flight Range Finding," IEEE Sensors journal, Vol. 16, no. 6, pp.1628-1633, 2016.

[13] S. Jahromi, J. Jansson, I. Nissinen, J. Nissinen and J. Kostamovaara, "A Single Chip Laser Radar Receiver with a 9x9 SPAD Detector Array and a 10-Channel TDC," Proceedings of the ESSCIRC'15, Graz, Austria, pp. 364-367, Sep. 14-18, 2015.

[14] S. Jahromi, J.-P. Jansson and J. Kostamovaara, "Solid-state 3D imaging using a 1nJ/100ps laser didoe transmitter and a single photon receiver matrix," Optics Express, vol.24, no.19, pp.21619-21632, 2016.

[15] D. Contini, F. Martelli and G. Zaccanti, "Photon migration through a turbid slab described by a model based on diffusion approximation. I. Theory," Applied optics, vol.36, no.19, pp.4587-4599, 1997.

[16] H. Wabnitz et al., " Performance assessment of time-domain optical brain imagers, part 2: nEUROPt protocol," Journal of Biomedical Optics, vol.19, no.8, 086012, 2014.